Journal of Trace Elements and Minerals 2 (2022) 100009

Contents lists available at ScienceDirect

Journal of Trace Elements and Minerals

journal homepage: www.elsevier.com/locate/jtemin

Effects of gallic acid on the nanocrystalline hydroxyapatite formation using the neutralization process

S. Jerdioui[a,*], L.L. Elansari[a], Nidal Jaradat[b,*], S. Jodeh[c,*], K. Azzaoui[a], B. Hammouti[a], M. Lakrat[a], A. Tahani[a], C. Jama[d], F. Bentiss[e]

[a] Laboratory of Applied Chemistry and Environment (LCAE). Department of Chemistry, Faculty of Sciences, University Mohamed I, Oujda, Morocco
[b] Faculty of Medicine and Health Sciences, An-Najah National University, P.O. Box 7 Nablus, Palestine
[c] Department of Chemistry, An-Najah National University, P.O. Box 7 Nablus, Palestine
[d] Univ. Lille, CNRS, INRAE, Centrale Lille, UMR 8207 - UMET - Unité Matériaux et Transformations, F-59000 Lille, France
[e] Laboratoire de Catalyse et de Corrosion des Matériaux (LCCM), Faculté des Sciences, Université Chouaib Doukkali, B.P. 20, M-24000 El Jadida, Morocco

ARTICLE INFO

Keywords:
Hydroxyapatite nanoparticles
Gallic Acid, Adsorption-desorption isotherms
XPS surface analysis
Bone tissue regeneration

ABSTRACT

Background: Hydroxyapatite nanoparticles (nHAp) have excellent properties, such as biocompatibility and osteoconductivity, which are critical for bone reconstruction. However, they remain inactive against pathogenic bacteria that can grow in defected bone tissue, and their use in some patients may result in some undesirable inflammatory reactions. Gallic acid (GA) is known for its specific anti-inflammatory and antibacterial properties. Coupling these characteristics with nHAp is of great interest.

Methods: The present study investigated the preparation of nHAp in the presence of various proportions of GA (0, 0.6, 2.5, and 5 mMol) using the neutralization method at room temperature. The effect of GA on the crystallinity, chemical composition, and surface specific area (SSA) of the prepared nHAp-GA composites was also studied.

Results: X-ray diffraction and Brunauer-Emmett-Teller (BET) analysis revealed that the precipitation of nHAp in the presence of a low fraction of GA induced the formation of nHAp with low crystallinity and high SSA (142 m^2/g), while GA at high concentration limited nHAp growth and favored the ACP formation with low SSA (32 m^2/g). X-ray photoelectron spectroscopy (XPS) indicated that GA is adsorbed on the nHAp surface and controlled its growth.

Conclusion: Overall, the prepared nHAp/Ga composites presented chemical and structural characteristics close to those of natural bone that make them a good candidate for bone tissue regeneration.

1. Introduction

Hydroxyapatite nanoparticles are calcium phosphate materials that play an important role in bone tissue regeneration due to their similarity to the inorganic part of the native bone [1]. This explains their excellent biocompatibility and osteoconductivity, as well as their ability to bond directly to living tissues [2]. Consequently, nHAp has been proposed for a broad range of clinical applications, especially for dentistry and orthopedics, as well as metallic implant coating [3]. Recently, nHAp is attracting more attention as a drug delivery system (DDS) for the local and controlled release of biologically active compounds [4]. nHAp can be combined with a variety of bioactive molecules, including anti-inflammatory, antimicrobial, antioxidant, and anticancer drugs, to create some promising DDS for treating infected bone tissue directly [5]. For many years, the attention focused on synthetic molecules to be combined with nHAp to treat several diseases after implantation. Recently, the application of natural molecules commonly extracted from plants has attracted more attention in the pharmaceutical area because of their many advantages [6]. Gallic acid (GA: $C_7H_6O_5$) is a phenolic acid that is mostly identified in fruits such as grapes, bananas, avocado, mango strawberries, oak bar, the leaves of bearberry, and green tea [7]. GA has been widely exploited for its biological benefits, including its anti-inflammatory, antiviral, and antibacterial properties [8,9]. Additionally, its anticancer activity has been proven against ovarian [10], lung [11], prostate [12], and breast cancer cells [13]. Therefore, coupling GA properties with nHAp for bone regeneration is highly preferred and recommended. The choice of this molecule is justified on the one hand by their biological activities such as anti-inflammatory, antioxidant, and antifungal and on the other hand by their well-defined size and their carboxyl and hydroxyl functions. The preparation of such compos-

* Corresponding authors.
E-mail addresses: souhailjjerdioui0@gmail.com (S. Jerdioui), nidaljaradat@najah.edu (N. Jaradat), sjodeh@najah.edu (S. Jodeh).

https://doi.org/10.1016/j.jtemin.2022.100009
Received 11 May 2022; Received in revised form 1 July 2022; Accepted 11 July 2022
Available online 15 July 2022

Table 1
Quantities of reagents used in the preparation of nHAp-GA samples.

Samples	GA (mol)	Ca $(OH)_2$ (mol)	H_3PO_4 (mol)
nHAp	-	0.024	0.0144
nHAp-GA_1	0.6×10^{-3}	0.024	0.0144
nHAp-GA_2	2.5×10^{-3}	0.024	0.0144
nHAp-GA_3	5×10^{-3}	0.024	0.0144

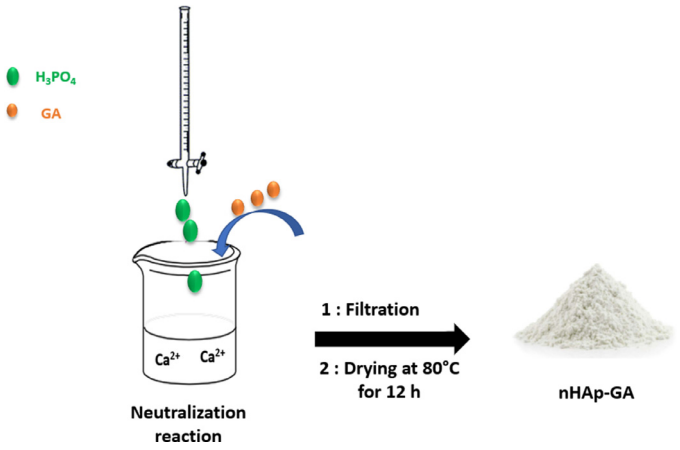

Scheme 1. Preparation of nHAp-GA composites using neutralization reaction.

ite (nHAp/GA) was mainly performed using two methods; adsorption on pre-prepared particles or incorporation during hydroxyapatite precipitation [14]. However, to the best of our knowledge, the neutralization method using calcium hydroxide $Ca(OH)_2$ and phosphoric acid H_3PO_4 as precursors has not been reported for the preparation of nHAp and GA composites. In the present study, the chemical and physical properties of precipitated Hap/GA samples are evaluated and compared to the obtained results with Hap/GA composites elaborated through other chemical routes. The specific goal was to use this simple preparation method for the precipitation of hydroxyapatite nanoparticles in the presence of GA and then characterize the obtained samples.

2. Materials and methods

All reagents used in the present work were received from Sigma-Aldrich (Germany) and utilized without further purification.

2.1. Preparation of nHAp-GA samples

The synthesis method adopted in this study to elaborate nHAp-GA composite samples was neutralization. As a calcium source, freshly prepared $Ca(OH)_2$ from CaO dispersed in distilled water (DW) was used, and phosphoric acid (H_3PO_4) was used as a phosphorus source.

For the preparation of nHAp, 0.014 M phosphoric acid was slowly added to 0.024 M calcium solution, and 0.5 M ammonium hydroxide solution (NH_4OH) was added when necessary to maintain the pH around 8. nHAp–GA composites with different amounts of GA were prepared using the same operative conditions,. GA was added to the Ca(OH) solution and stirred for 1 h before adding the H_3PO_4 solution dropwise. Three nHAp–GA samples were synthesized as given in Table 1 and Scheme 1. The resulting solutions were stirred for an additional 2 h before being filtrated and washed twice with DW before being dried overnight at 80°C.

In the following, we designated the precipitated samples nHAp as nHAp-GA_1, nHAp-GA_2, and nHAp-GA_3 according to the GA amount as indicated in Table 1.

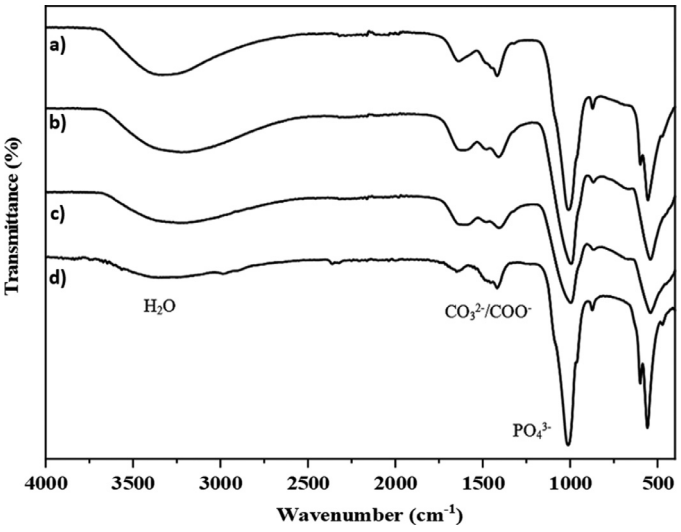

Fig. 1. FTIR spectra of the prepared samples, a: nHAp-GA_1; b: nHAp-GA_2, c: nHAp-GA_3, and d: nHAp.

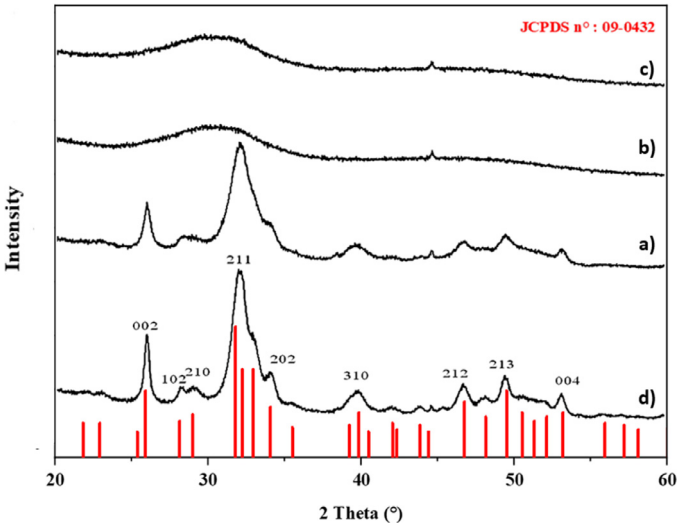

Fig. 2. XRD pattern of the prepared samples; a: nHAp-GA_1, b: nHAp-GA_2, c: nHAp-GA_3, and d: nHAp.

2.2. Characterization of synthesized samples

Fourier transform infrared spectroscopy (FTIR) was performed to characterize the chemical functional groups of prepared powders suspended in KBr pellets using a Shimadzu FT-IR 8400S series instrument (Shimadzu, Japan). The FTIR spectra were acquired from 4000 to 400 cm^{-1} at a data acquisition rate of 4 cm^{-1}.

The crystalline phase of synthesized samples was evaluated by X-ray diffraction (XRD) using a Shimadzu (XRD Shimadzu 6000) diffractometer with nickel-filtered Cu-Kα radiation (1.5418A°). The characterization was operated at 30 mA and 40 kV, with a scanning 2θ range between 10° and 60° and a step size of 0.02°. Thermogravimetric analysis (TGA) was carried out utilizing Shimadzu DTG-60 to evaluate the thermal behavior of the paper powders. Samples were heated up to 900°C with a heating speed of 10°C /min in a nitrogen atmosphere. Scanning electron microscopy (SEM) was adopted to observe the morphology of the sample using a HIROX SH-5500P Benchtop instrument. Elemental analysis of the prepared samples was determined by employing inductively coupled plasma optical emission spectrometry (ICP-OES). The specific surface area (SSA) and pore size were respectively

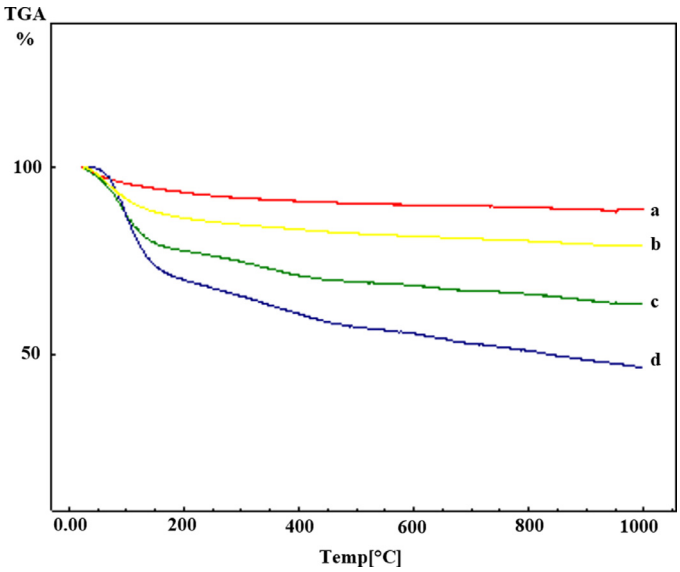

Fig. 3. TGA curves of the prepared samples with different proportions of GA, a: nHAp-GA_3, b: nHAp-GA_2, c: nHAp-GA_1, and d: nHAp.

determined by the Brunauer–Emmett–Teller (BET) and Barrett–Joyner–Halenda (BJH) methods using Autosorb 1 Instruments. An X-ray Photoelectron Spectroscopy (XPS) surface analysis was conducted using a KRATOS AXIS ULTRA DLD spectrometer. The values of the binding energies (Ca 2p, O 1s, P 2p, C 1s, N 1s, and Mg 2s) associated with the superficial layers of prepared samples were recorded using Al Kα radiation (hv = 1486,6 eV).

3. Results and discussion

3.1. Characterization of prepared samples

The FTIR spectra of the prepared samples processed by different GA rates are shown in Fig. 1. The existence of organic and inorganic phases in all composites was validated. In all spectra, characteristic absorption bands of phosphate groups (PO_4^{3-}) in hydroxyapatite were observed at 566, 603, 961, and 1036 cm^{-1} [15]. The vibrational band at pure nHAp near 1420 cm^{-1} represents carbonate ions (CO_3^{2-}), indicating that the prepared sample was carbonated hydroxyapatite [16].

The large absorption band situated between 2600 and 3800 cm^{-1} and the small band at 1630 cm^{-1} suggested the presence of water molecules in the prepared composites [17]. Additionally, typical bands of GA in the composite samples were observed between 1350 and 1600 cm^{-1}, which was associated with the vibration band of C-O or C=O groups [18]. The intensity of these bands increased as the GA amount became more important for nHAP-GA_2 and c: nHAP-GA_3, respectively, while a decrease in the intensity of the phosphate bands was noticed. XRD analysis of synthesized samples at different rates of GA is presented in Fig. 2.

The obtained XRD patterns indicated a noticeable change in the sample's crystallinity due to the accumulation of GA. On the one hand, nHAp and nHAp-GA_1 samples' XRD patterns showed characteristic diffraction planes of a poorly crystallized hydroxyapatite in the hexagonal crystal system (JCPDS # 09-0432) [19]. On the other hand, nHAp-GA_2 and nHAp-GA_3 exhibited patterns of amorphous calcium phosphate. This result suggested that the GA significantly influenced the crystallinity of nHAp and limited its crystal growth. In fact, according to their chemical structures, polyphenol acids play an important role in hydroxyapatite precipitation and can slow or inhibit the growth of Hap particles [20]. In support of the present study, Tang et al. [18] also reported that

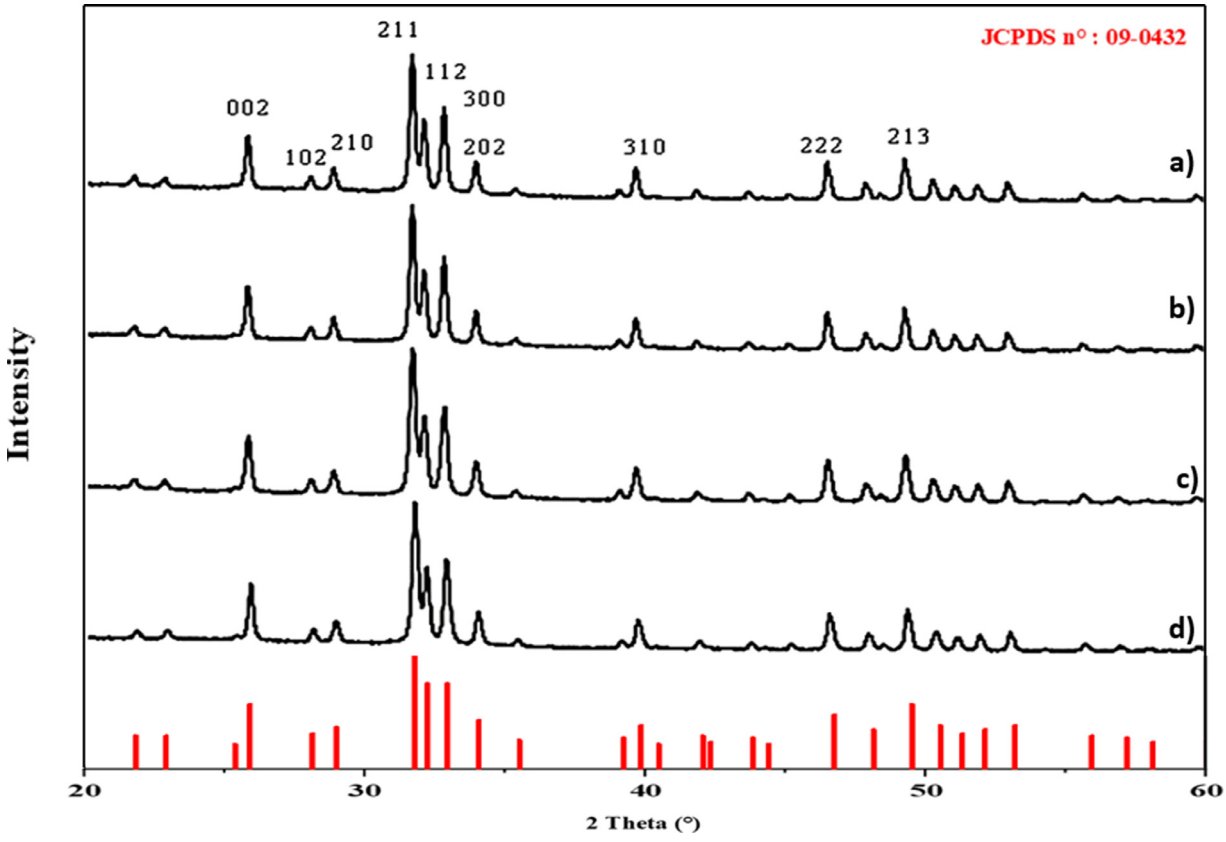

Fig. 4. XRD pattern of the synthesized samples heated at 900°C a: nHAp-GA_3, b: nHAp-GA_2, c: nHAp-GA_1, and d: nHAp.

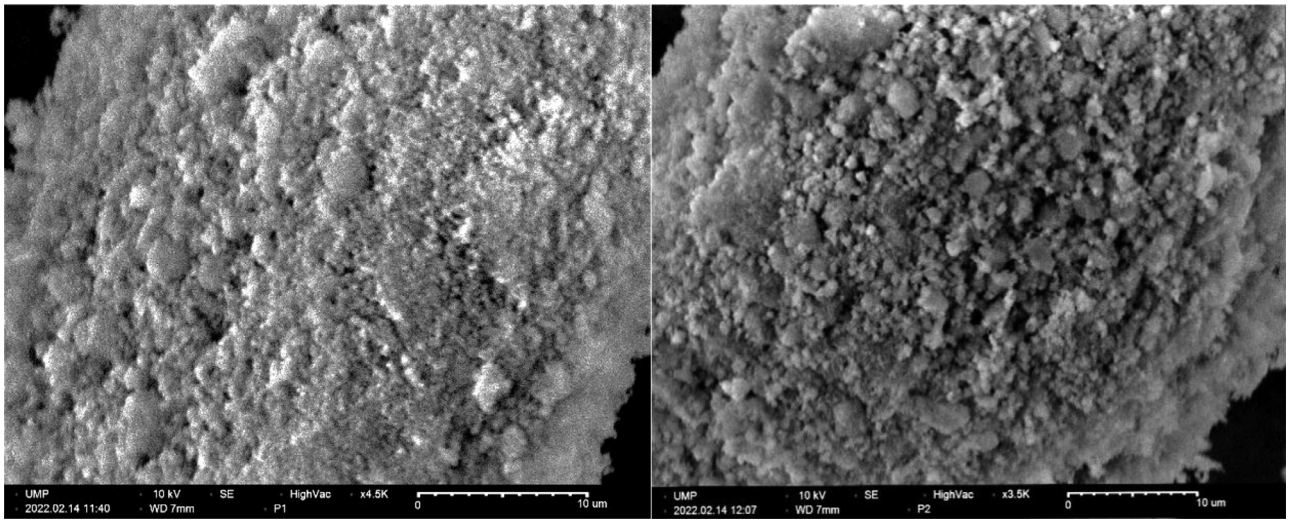

Fig. 5. SEM images of nHAp and nHAp-GA_3 samples

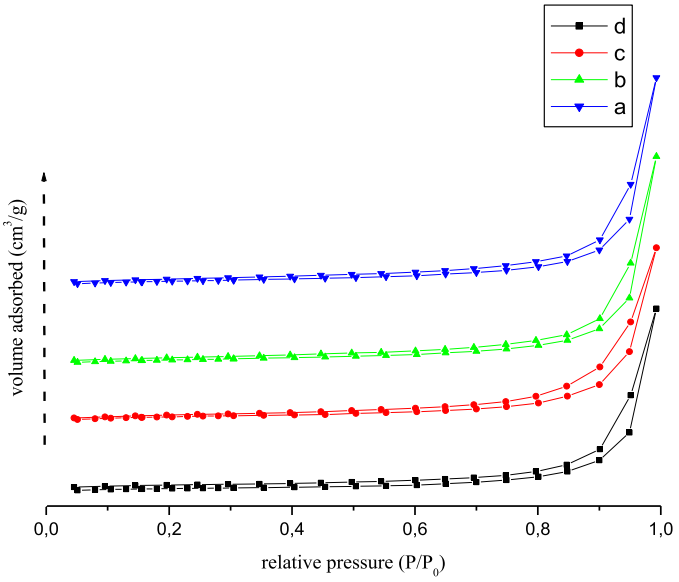

Fig. 6. The pore distribution of the prepared samples, a: nHAp, b: nHAp-GA_3, and nHAp-GA_1.

GA slower the hydroxyapatite formation and limits its crystal growth in the (002) directions. This could be attributed either to the interaction between GA and calcium ions Ca^{2+} during nHAp precipitation or to GA adsorption on the nHAp surface. Additionally, Palierse et al. [21] observed that at low proportion, polyphenol did not alter the shape and particle size of hydroxyapatite. However, the presence of an important amount of polyphenols during nHAp precipitation could inhibit its formation and results in highly amorphous calcium particles, which are in accordance with our results. Consequently, these findings suggest that GA could be employed to control the crystallinity of nHAp during the synthesis process. Moreover, it seems that no matter the precursor used earlier; ($CaCl_2/KH_2PO_4$) [18], ($Ca(NO_3)_2/NH_4H_2PO_4$) [22] or herein; ($CaOH/H_3PO_4$), for Hap preparation, the presence of an important amount of GA favors the formation of amorphous calcium–phosphate and inhibit the HAp nucleation. The TGA diagrams of samples prepared in aqueous media in the presence of GA are represented in Fig. 3. In all diagrams, we observed a gradual mass loss with three stages.

Table 2
Specific surface area, pore volume, and pore size of precipitated samples.

Sample	Specific surface (m^2/g)	Pore volume (cc/g)	Rays of the pores (A°)
nHAp-GA_3	31.037	0.251	89.31
nHAp-GA_2	32.117	0.256	87.845
nHAp-GA_1	142.254	0.279	15.368
nHAp	85.705	0.325	24.330

The first loss is recorded between 25 and 200°C, corresponding to the removal of adsorbed water on the apatite surface. The second step, between 200°C and 600°C, is attributed to the decomposition of the organic phase and carbonate ions [23]. This mass loss increases gradually as the concentration of GA becomes important. The last mass loss is observed beyond 650°C attributed to the structural transformation of groups phosphate, namely the reaction of the OH^- ions of the apatite with $P_2O_7^{2-}$ ions [24].

$$2\ HPO_4^{2-} \rightarrow P_2O_7^{2-} + H_2O(200°C–500°C).$$

and

$$P_2O_7^{2-} + 2\ OH^- \rightarrow 2\ PO_4^{3-} + H_2O\ (700\text{-}800°C).$$

At high temperatures, we are witnessing a complete elimination of the organic phase and formation of well-crystallized hydroxyapatite $Ca_{10}(PO_4)_6(OH)_2$, as presented in Fig. 4.

To observe the morphology of nHAp and nHAp-GA_3 samples, scanning electron microscopy (SEM) analysis was used.

As shown in Fig. 5a, the morphology of pure nHAp presented is mainly formed by a spherical agglomerate with a heterogeneous surface. The SEM image of nHAp-GA_3 is provided in Fig. 5b showed large particles compared to nHAp, meaning that GA was responsible for particle agglomeration.

It was interesting to evaluate the effect of GA on the specific surface area, pore-volume, and rays of pores of precipitated samples. The Brunauer-Emmett-Teller (BET) theory method is usually used to study the texture of the samples and determine their surface area, while the BJH desorption method is used to estimate the total pore volume of the sample [25]. The BET/BJH results reported in Table 2 were obtained from the results of Figs. 6 and 7.

Table 2 demonstrates the important effect of GA on the surface properties of precipitated samples.

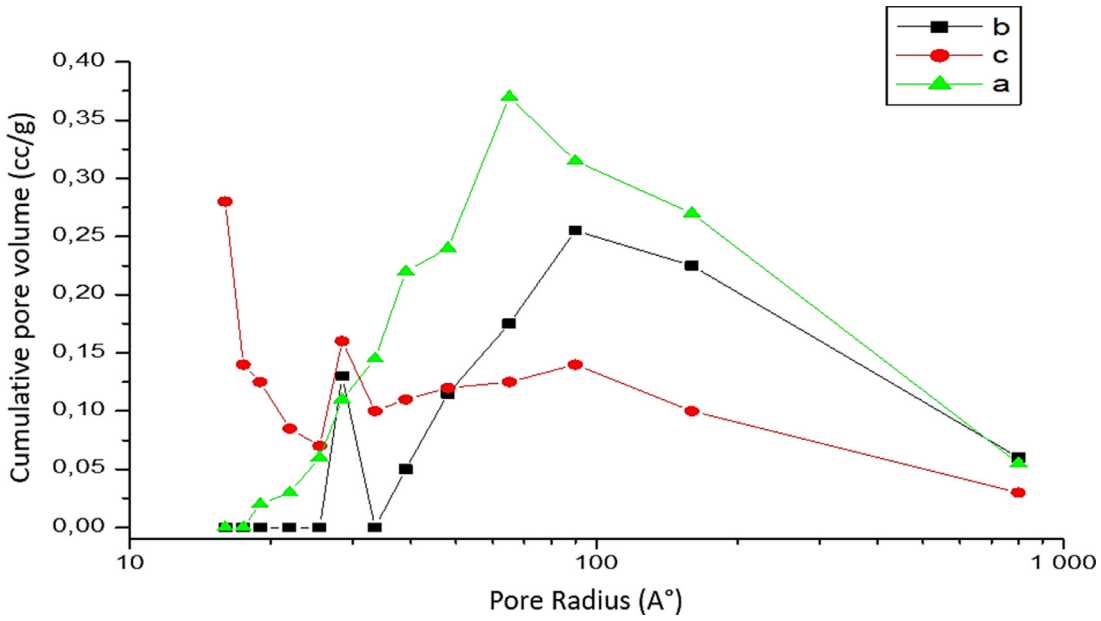

Fig. 7. Isothermal adsorption-desorption of N2 on prepared samples. a: nHAp, b: nHAp-GA1, c: nHAp-GA2, and d: nHAp-GA3.

The measurement of the SSA of the apatite samples showed different values depending on the GA initially rate introduced into the reaction mixture. The precipitation of nHAp in the presence of a small amount of GA was responsible for an increase in the specific surface area and a decrease in the pore volume and pore size compared to that of pure nHAp. Accordingly, the SSA increased significantly from 85.70 m^2g^{-1} for nHAp to 142.25 m^2 g^{-1} for the nHAp-GA_1 sample while the pore volume and pore size decreased respectively from 0.325 cc/g and 24.330 A° to 0.279 cc/g and 15.368 A°. This was expected since this latter presented a structure with low crystallinity compared to the pure nHAp, which means a small crystallite size and consequently large SSA. On the other hand, a significant decrease in the SSA with an increase in the volume pore is noticed when the GA amount becomes important during nHAp precipitation. The low value of SSA was obtained in the case of nHAp-GA_3, which reached 31.037 m^2/g. This decrease was accompanied by an increase in the pore diameter (89.31 A°). The reason behind this behavior could be attributed to the complex character of the GA during its deposition on the hydroxyapatite surface that partially fills its large pores.

Fig. 7 highlighted the nitrogen adsorption-desorption isotherm for the prepared samples with different rates of gallic acid. The isotherms obtained are characterized by a gradual increase in the quantity adsorbed as a function of the equilibrium pressure relative to values of (P/P0) greater than 0.6. For lower pressures, the isotherm is characterized by a saturation level, characteristic of mesoporous adsorbents in which there is capillary condensation. The process of desorption, in this case, is not reversible; it is characterized by hysteresis of desorption concerning adsorption. The isotherm thus observed is of type IV according to the IUPAC classification (26), characteristic of adsorption in the mesopores. At low pressure, the adsorption is stronger in the micropores due to the strong gas-solid interaction. The form of the adsorption-desorption isotherms remains the same with different rates of gallic acid, which indicates that the nature of the pores remains the same.

Additionally, it was clear from BJH pore size distribution curves (Fig. 6) that the prepared powders contained mainly mesopores with a size ranging from 8 to 20 nm.

To highlight the effect of adding this bioactive molecule (GA) on the chemical formula of precipitated apatite samples, we measured the major elements constituting the prepared composites, such as Calcium and Phosphorus, using ICP analysis (Table 3). The findings revealed that

Table 3
ICP analysis of prepared composites.

Sample	Ca (mg/L)	P (mg/L)	Ca/P
nHAp-GA_3	264.54	110.18	1.85
nHAp-GA_2	272.12	114.25	1.84
nHAp-GA_1	311.38	132.65	1.81
nHAp	332.21	152.68	1.677

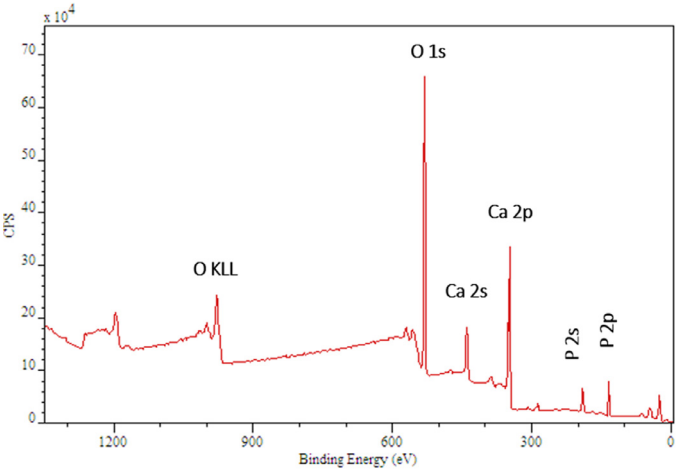

Fig. 8. XPS survey spectrum measured of nHAp.

the Ca/P ratio for all samples was equal to or higher than the theoretical value (1.677) of stoichiometric hydroxyapatite.

Particularly, the results indicated that the hydroxyapatite prepared in the absence of GA is stoichiometric with a molar ratio Ca/P of 1.677. Moreover, we observed that the calculated Ca/P ratio of all composites increased as a function of the GA rate initially introduced. This variation can be attributed to the presence of a higher concentration of Ca^{2+} at the surface of nHAp/GA composites that mainly occurred through the reaction of GA and calcium ions during sample precipitation. It is well known that phenols with their functional groups have a strong affinity

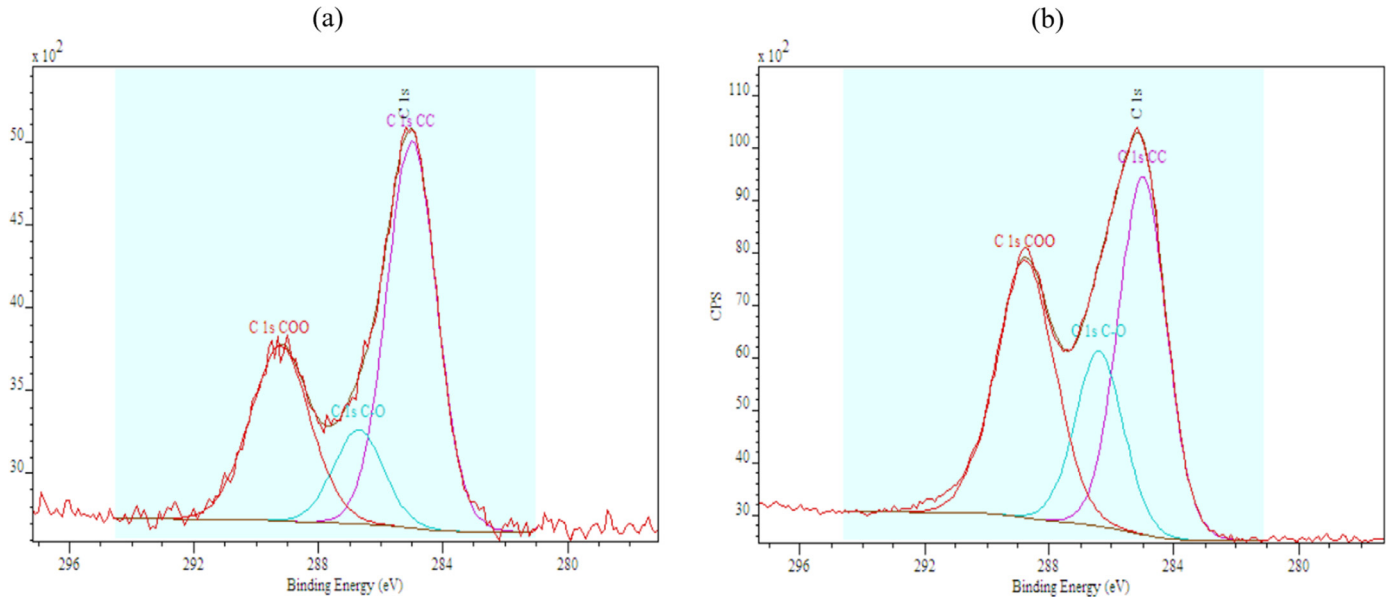

Fig. 9. XPS high-resolution spectra of C 1s for a: nHAp and b: nHAp-GA_3.

Table 4
Binding energies and atomic percentage of elements Ca 2p, O 1s, P 2p, and C 1s for nHap and nHAp-GA_3 obtained from XPS analysis.

Sample	Binding Energy (eV)				Atomic (%)			
	P 2p	Ca $2p_{3/2}$	O 1s	C 1s	P 2p	Ca $2p_{3/2}$	O 1s	C 1s
HAp	133.4	347.1	531.1	285.2	12.7	18.8	61.3	6.9
HAp + GA_3	133.2	347.3	531.2	285.2	8.2	13.9	52.9	23.4

to the hydroxyapatite surface. These features are allowed antibiotic and anti-inflammatory molecules to bind to hydroxyapatite [26,27].

X-ray photoelectron spectroscopy (XPS) analysis was adopted to verify the GA deposition at the nHAp surface and determine the nature and binding type of the two phases. To analyze the feasibility of the treatment performed by the GA deposition at the nHAp surface, after 6 h of treatments, the surface morphology of the nHAp was studied using FE-SEM (field-emission scanning electron microscope) with double beam (Helios Nanolab 650 de FEI Company, Oxford, UK).The X-ray photoelectron (XPS) analysis were performed on a Physical Electronic PHI Versa Probe II spectrometer via monochromatic Al-Kα (49.1 W, 15 kV, and 1486.6 eV), and the central signals of the interest elements were analyzed with a hemispheric multi-channel detector. The spectra of the samples were registered with constant passage energy of 29.35 eV with a circular surface area of 200 μm diameter. The resulting XPS spectra were examined by the PHI Smart software and treated by MultiPak 9.3 software package. The signal of the incidental carbon C 1*s* (285.2 eV) references the binding energy, which is determined from the Background Shirley and Gauss-Lorentz plots.

Using this analytical technique, we determined in Table 4, the binding energies of the major constituents (Ca 2p, O 1s, P 2p, and C 1s) are associated with the superficial layers of our apatite samples and the atomic ratio.

Calcium, phosphorus, and oxygen are connected to the nHAp structure (Fig. 8), while the high percentage of carbon is connected to the chemical composition of gallic acid.

For both samples, the measured Binding Energy (BE) of P_{2p} (133.4 eV), Ca $2p_{3/2}$ (347.1 eV), and O 1s (531eV) are in good agreement with XPS studies on Hap [28,29]. The presence of the C 1s peak at approximately 285.0 eV can probably be due to surface contamination that occurred during experimental conditions.

Concerning the percentage atomic, the addition of GA significantly increases the carbon content, indicating the existence of phenolic compounds. The surface of the nHAp-GA_3 composite is mainly contained P, O, Ca, and C, according to the nHAp composition. On the other hand, the percentage of the three main constituents of HAp (calcium, phosphorous, and oxygen) was decreased, which is attributed directly to the presence of the organic acid on its surface.

The carbon decomposition results and especially the two components C 1s (C-O) and C 1s (O-C = O) are given in Table 5. We observed that the atomic % of both components increased significantly and reached respectively 20.7 % and 37.2 % with the addition of GA, as also observed in Fig. 9a and b.

In the case of nHAp treated with GA (Fig. 10a and b), there is a decrease in the atomic % of oxygen linked to a single phosphorus atom and/or atomic % of oxygen bonded to the carbonate, which reaches up to 67.4%. At the same time, an increase in the atomic percentage of oxygen O1s (-OH)/(C-O) takes a value of 32.6 % (Table 5).

Overall, GA contains carboxylic functions and three hydroxyl groups and their adsorption to the nHAp surface increased the atomic percentage of oxygen O 1s (-OH)/(C-O), C 1s (C-O), and (O-C=O).

Looking at the main results of the present study, it can be stated that nHAp was successfully precipitated in the presence of GA using the wet neutralization method. In fact, through this synthesis process, we demonstrated that apatite adsorbs organic acids; this can be explained by an interaction between surface Ca^{2+} cation and acidic groups of GA. Furthermore, we observed that GA could control the crystallinity and crystal growth of nHAp as well as its surface specific, pore size, and pore volume.

All the results obtained by X-ray diffraction analysis and by infrared spectroscopy confirm the formation of a poorly crystallized apatitic phase; once calcined at 900°C, the crystallinity of the phase becomes better.

Table 5
Binding energies and atomic percent % carbon for the C 1s and O 1s core lines for nHAp and nHAp-GA_3.

Sample	Carbon decomposition					
	Binding energy (eV)			Atomic %		
	C1s (C-C)	C1s (C-O)	C1s (COO)	C1s (CC)	C1s (C-O) C_{1s}(1)	C1s (COO) C_1s(2)
nHAp	285.0	286.7	289.2	56.1	13.7	30.3
Hap-GA_3	285.0	286.4	288.8	42.1	20.7	37.2
	Oxygen Decomposition					
	Binding energy (eV)			Atomic %		
	O1s (PO_4/CO_3)	O1s (-OH/C-O)		O1s (PO_4/CO_3) O_1s(2)	O1s (-OH/C-O) O_{1s}(1)	
nHAp	531.1	532.6		82.0	18.0	
nHap-GA_3	531.1	532.4		67.4	32.6	

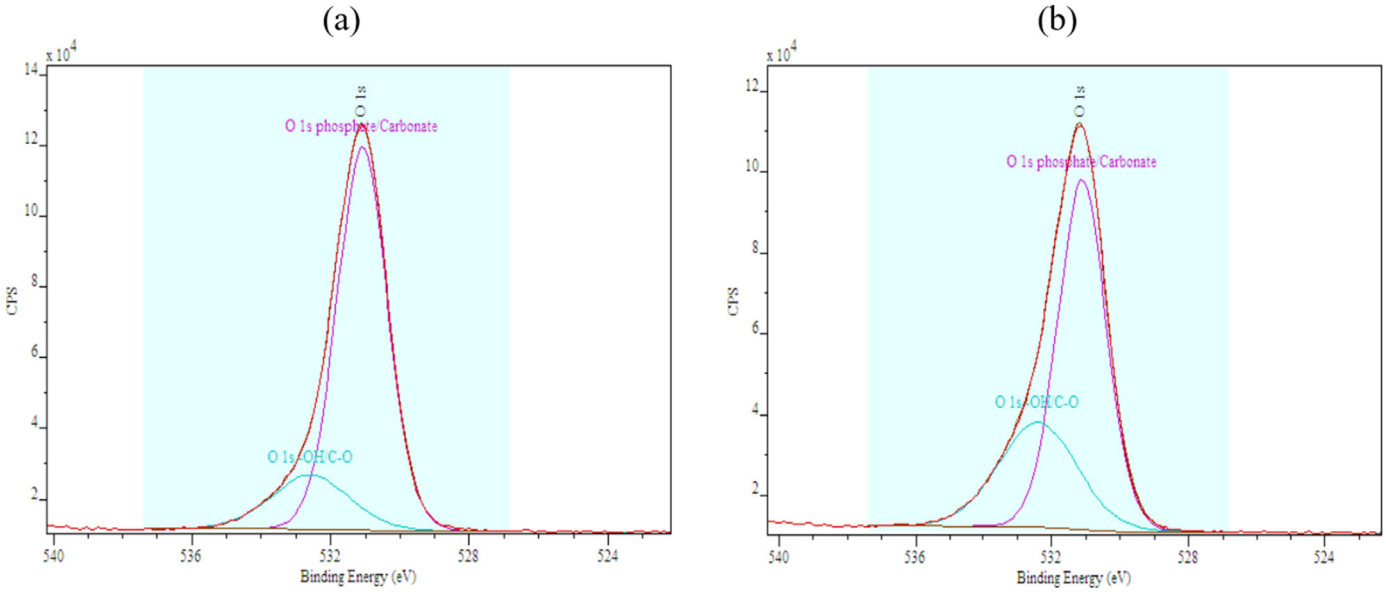

Fig. 10. High-resolution X-ray photoelectron of O 1s for a: nHAp and b: HAp-GA_3.

The specific surface decreases significantly with the increase in the rate of this organic molecule; the low values of the specific surface are obtained in the case of the prepared product (HAp + 5 10^{-3} mol G.A) and which reaches 31,037 m^2 /g.

We note that the Ca/P atomic ratio measured varies according to the level of acid initially introduced. For the various samples, the constituent elements of $Ca_{10}(PO_4)_6(OH)_2$ are found at the same energies. For these samples, the apatite is not modified on the surface. Calcium is in oxidation state +2 and phosphorus in phosphate form in oxidation state +5. The acid does not affect the oxidation state of the various constituents of apatite. All the results were gathered to show that there is an adsorption of this phenolic acid on our apatitic matrix.

Conclusion

In this study, nHAp was prepared in the presence of different proportions of GA using the neutralization method. The effect of the GA amount introduced on the chemical and structural characteristics of nHAp during its formation was elucidated. Through this investigation, we demonstrated that GA controlled the nucleation process of nHAp. Accordingly, XRD results highlighted significant changes in the nHAp crystallinity as a function of the GA rate initially introduced. In fact, nHAp with a low GA rate showed the formation of a poorly crystallized hydroxyapatite, whereas a higher GA rate favored amorphous calcium precipitation. This is justified by the interaction between functional groups of GA and surface Ca^{2+} in the nHAp, as confirmed by XPS analysis. The specific surface area of prepared samples was also influenced by GA, which increased when a small amount was introduced and significantly decreased with an increase in the rate of this organic molecule. Overall, the nHAp-GA composites present interesting characteristics such as low crystallinity, small crystallite size, as well as antibacterial and anti-inflammatory properties provided by GA that make them useful substitute materials for dentistry, orthopedic applications, and drug delivery systems.

Funding

The work that resulted in this article did not have financial support.

Declaration of Competing Interest

The authors declare that they have no known competing financial interests or personal relationships that could have appeared to influence the work reported in this paper.

CRediT authorship contribution statement

S. Jerdioui: Methodology, Conceptualization, Software. **L.L. Elansari:** Methodology, Conceptualization, Software. **Nidal Jaradat:** Data curation, Formal analysis, Writing – original draft, Writing – review & editing. **S. Jodeh:** Data curation, Formal analysis, Writing – original draft, Writing – review & editing. **K. Azzaoui:** Methodology,

Conceptualization, Software. **B. Hammouti:** Methodology, Conceptualization, Software. **M. Lakrat:** Methodology, Conceptualization, Software. **A. Tahani:** Methodology, Conceptualization, Software. **C. Jama:** Methodology, Conceptualization, Software. **F. Bentiss:** Methodology, Conceptualization, Software.

Acknowledgments

The authors would like to thank Mohammed 1st University, An-Najah National University, Université Lille I, and Université Chouaib Doukkali.

References

[1] Y.W. Sari, A. Tsalsabila, N. Darmawan, Y. Herbani, Hydroxyapatite formation under calcium-deficient concentration conditions modulated by amino acid-capped gold nanoparticles, Ceram. Int. 48 (2022) 13665–13675.
[2] M. Fathi, A. Hanifi, V. Mortazavi, Preparation and bioactivity evaluation of bone-like hydroxyapatite nanopowder, J. Mater. Process. Technol. 202 (2008) 536–542.
[3] S.V. Dorozhkin, Dental applications of calcium orthophosphates (CaPO4), J. Dent. Res. 1 (2) (2019) 1007.
[4] S. Lara-Ochoa, W. Ortega-Lara, C.E. Guerrero-Beltrán, Hydroxyapatite nanoparticles in drug delivery: physicochemistry and applications, Pharmaceutics 13 (10) (2021) 1642.
[5] M.U. Munir, S. Salman, I. Javed, S.N.A. Bukhari, N. Ahmad, N.A. Shad, F. Aziz, Nano-hydroxyapatite as a delivery system: overview and advancements, Artif. Cells Nanomed. Biotechnol. 49 (1) (2021) 717–727.
[6] A.G. Muller, S.D. Sarker, I.Y. Saleem, G.A. Hutcheon, Delivery of natural phenolic compounds for the potential treatment of lung cancer, DARU J. Pharm. Sci. 27 (1) (2019) 433–449.
[7] K. Essifi, M. Lakrat, D. Berraaouan, M.-L. Fauconnier, A. El Bachiri, A. Tahani, Optimization of gallic acid encapsulation in calcium alginate microbeads using Box-Behnken Experimental Design, Polym. Bull. 78 (10) (2021) 5789–5814.
[8] S. Arunkumar, K. Ilango, R. Manikandan, N. Ramalakshmi, Synthesis and anti-inflammatory activity of some novel pyrazole derivatives of gallic acid, E- J. Chem. 6 (S1) (2009) S123–S128.
[9] K. Rajamanickam, J. Yang, M.K. Sakharkar, Gallic acid potentiates the antimicrobial activity of tulathromycin against two key bovine respiratory disease (BRD) causing–pathogens, Front. Pharmacol. (2019) 1486.
[10] Z. He, X. Liu, F. Wu, S. Wu, G.O.N. Rankin, I. Martinez, Y. Rojanasakul, Y.C. Chen, Gallic acid induces S and G2 phase arrest and apoptosis in human ovarian cancer cells in vitro, Appl. Sci. 11 (9) (2021) 3807.
[11] D.Y. Kang, N. Sp, E.S. Jo, A. Rugamba, D.Y. Hong, H.G. Lee, J.-S. Yoo, Q. Liu, K.-J. Jang, Y.M. Yang, The inhibitory mechanisms of tumor PD-L1 expression by natural bioactive gallic acid in non-small-cell lung cancer (NSCLC) cells, Cancers 12 (3) (2020) 727.
[12] Y.-G. Jang, E.-B. Ko, K.-C. Choi, Gallic acid, a phenolic acid, hinders the progression of prostate cancer by inhibition of histone deacetylase 1 and 2 expression, J. Nutr. Biochem. 84 (2020) 108444.
[13] H.-L. Lee, C.-S. Lin, S.-H. Kao, M.-C. Chou, Gallic acid induces G1 phase arrest and apoptosis of triple-negative breast cancer cell MDA-MB-231 via p38 mitogen-activated protein kinase/p21/p27 axis, Anti-cancer Drugs 28 (10) (2017) 1150–1156.
[14] C. Stötzel, F. Müller, F. Reinert, F. Niederdraenk, J. Barralet, U. Gbureck, Ion adsorption behaviour of hydroxyapatite with different crystallinities, Colloids Surf. B 74 (1) (2009) 91–95.
[15] M. Lakrat, S. Fadlaoui, M. Aaddouz, O. El Asri, M. Melhaoui, M. El Miloud, Synthesis and characterization of composites based on hydroxyapatite nanoparticles and chitosan extracted from shells of the freshwater crab Potamon algeriense, Prog. Chem. Appl. Chitin. Deriv. 25 (2020) 132–142.
[16] K. Azzaouia, E. Mejdoubia, A. Lamhamdia, M. Lakrata, O. Hamedb, S. Jodehb, M. Berrabaha, A. Elidrissic, I. El Meskinid, M. Daoudid, Preparation of hydroxyapatite biobased microcomposite film for selective removal of toxic dyes from wastewater, Polymer 1 (27) (2019) 28.
[17] M. Lakrat, M. Jabri, M. Alves, M.H. Fernandes, L.L. Ansari, C. Santos, E.M. Mejdoubi, Three-dimensional nano-hydroxyapatite sodium silicate glass composite scaffold for bone tissue engineering-a new fabrication process at a near-room temperature, Mater. Chem. Phys. 260 (2021) 124185.
[18] B. Tang, H. Yuan, L. Cheng, X. Zhou, X. Huang, J. Li, Effects of gallic acid on the morphology and growth of hydroxyapatite crystals, Arch. Oral Biol. 60 (1) (2015) 167–173.
[19] C.F. dos Santos, P.S. Gomes, M.M. Almeida, M.-G. Willinger, R.-P. Franke, M.H. Fernandes, M.E. Costa, Gold-dotted hydroxyapatite nanoparticles as multifunctional platforms for medical applications, RSC Adv. 5 (85) (2015) 69184–69195.
[20] T.H. Aneem, S.K. Saha, R.A. Jahan, S.Y. Wong, X. Li, M.T. Arafat, Effects of organic modifiers and temperature on the synthesis of biomimetic carbonated hydroxyapatite, Ceram. Int 45 (18) (2019) 24717–24726.
[21] E. Palierse, S. Masse, G. Laurent, P. Le Griel, G. Mosser, T. Coradin, C. Jolivalt, Synthesis of hybrid polyphenol/hydroxyapatite nanomaterials: adsorption vs. in situ incorporation, Mater. Chem. 2021 (2021), doi:10.26434/chemrxiv-2021-39frr.
[22] B. Tang, H. Yuan, L. Cheng, X. Zhou, X. Huang, J. Li, Control of hydroxyapatite crystal growth by gallic acid, Dent. Mater. J. 2015 (2015) 2014–2175.
[23] S.-G. Choi, S.-S. Park, S. Wu, J. Chu, Methods for calcium carbonate content measurement of biocemented soils, J. Mater. Civ. Eng. 29 (11) (2017) 06017015.
[24] K. Tonsuaadu, K.A. Gross, L. Plūduma, M. Veiderma, A review on the thermal stability of calcium apatites, J. Therm. Anal. Calorim. 110 (2) (2012) 647–659.
[25] E.P. Barrett, L.G. Joyner, P.P. Halenda, The determination of pore volume and area distributions in porous substances. I. Computations from nitrogen isotherms, J. Am. Chem. Soc. 73 (1) (1951) 373–380.
[26] Y. Ryabenkova, N. Jadav, M. Conte, M.F. Hippler, N. Reeves-McLaren, P.D. Coates, P. Twigg, A. Paradkar, Mechanism of hydrogen-bonded complex formation between ibuprofen and nanocrystalline hydroxyapatite, Langmuir 33 (12) (2017) 2965–2976.
[27] G. Riccucci, M. Cazzola, S. Ferraris, V.A. Gobbo, M. Miola, A. Bosso, G. Örlygsson, C.H. Ng, E. Verne, S. Spriano, Surface functionalization of bioactive glasses and hydroxyapatite with polyphenols from organic red grape pomace, J. Am. Ceram. Soc. 105 (3) (2022) 1697–1710.
[28] V. Secchi, S. Franchi, M. Dettin, A. Zamuner, K. Beranová, A. Vladescu, C. Battocchio, V. Graziani, L. Tortora, G. Iucci, Hydroxyapatite surfaces functionalized with a self-assembling peptide: XPS, rairs and nexafs study, Nanomaterials 10 (6) (2020) 1151.
[29] M. Casaletto, S. Kaciulis, G. Mattogno, A. Mezzi, L. Ambrosio, F. Branda, XPS characterization of biocompatible hydroxyapatite–polymer coatings, Surf. Interface Anal. 34 (1) (2002) 45–49.